Importance of Low-Frequency Contributions to Eddy Fluxes Observed over Rough Surfaces

RICARDO K. SAKAI, DAVID R. FITZJARRALD, AND KATHLEEN E. MOORE

Atmospheric Sciences Research Center, University at Albany, State University of New York, Albany, New York

(Manuscript received 13 November 2000, in final form 5 July 2001)

ABSTRACT

Eddy covariance flux observations at a deciduous temperate forest site (83 days) and at a boreal forest site (21 days) are analyzed for midday periods (1100–1400 LT). Approximate stationarity of the time series is demonstrated, and the ensemble-averaged roughness sublayer cospectra are presented. Spectral and cospectral forms in the roughness sublayer are more peaked than those found in an inertial sublayer. They exhibit similar forms dependent on $(z - d)/(h - d)$, where d is the displacement height and h is the canopy height. The inertial-layer spectral forms are recovered when observations are made where this scaled height is approximately 4. For a sample summer at the midlatitude deciduous forest, large eddies with periods from 4 to 30 min contribute about 17% to surface eddy fluxes of heat, water vapor, and carbon dioxide (CO_2). Much larger contributions can occur in light-wind conditions. This effect, likely caused by the passage of convective boundary layer eddies, is not observed when using many currently popular averaging procedures. Several running-mean periods have been used to assess the effect of the mean removal procedure on flux estimates. Given the assumption that large eddies would have been sampled at the towers had an ensemble measurement been possible, a correction is proposed based primarily on the mean wind speed to adjust fluxes obtained using short averaging intervals. This correction is successful in achieving observational energy-balance closure at two dissimilar forested sites. Cospectral similarity is found for all scalars studied. Daytime fluxes of CO_2, for example, can be underestimated at standard flux towers by 10%–40%, depending on wind speed.

1. Introduction

Eddy covariance systems are used extensively to study turbulent transfer above plant canopies (Table 1). These measurements are usually made in a roughness sublayer (RSL), in which the turbulent flow is directly affected by the size of roughness elements [Kaimal and Finnegan 1994 (hereinafter KF94), p. 71]. Several recent studies discuss how the method of obtaining the mean quantities influences the flux estimates made at towers (e.g., Foken and Wichura 1996; Aubinet et al. 2000; Massman 2000; Rannik and Vesala 1999). The motivation for reexamining mean removal techniques stems from the fact that the observational surface energy balance often does not close when measurements are made over forests (Table 1). Aircraft measurements face similar difficulties in closing the energy budget. In the First International Satellite Land Surface Climatology Project Field Experiment in Kansas, Betts (1992) found large residuals in the heat and moisture budgets, which Grossman (1992) attributed in part to inadequate sampling of long-wavelength flux contributions. Lack of budget closure at towers might be explained by the use of different instruments and techniques to find the components in the surface-layer energy balance. For example, the source area (footprint) for the net radiative flux (''net radiation'' Q_*) is much smaller than the footprint of the eddy covariance system used to find turbulent heat and water vapor fluxes (Schmid 1997). Although this argument surely holds in many cases for which the underlying surface is heterogeneous, it seems an inadequate explanation for the uniform underestimation of the energy balance for the results presented in Table 1. We believe that the turbulent fluxes are being underestimated during convective conditions because the mean removal period used typically is too short to resolve larger eddies. The objective of this paper is to estimate how low-frequency fluctuations contribute to flux estimates and to develop a scheme to correct flux observations to account for what may be missed. To do this, we identify cospectral forms in the layer just above forest canopies in which most observations are made.

The balance of an energy budget in a layer is given by

$$A = -(Q_* - G) = H + \mathrm{LE} + \mathrm{St} + \mathrm{Adv}, \quad (1)$$

where upward fluxes are taken to be positive and A is the available energy flux [$A = -(Q_* - G)$; G is the soil heat flux]. The available energy can be partitioned

Corresponding author address: Ricardo K. Sakai, Atmospheric Sciences Research Center, University at Albany, SUNY, 251 Fuller Road, Albany, NY 12203.
E-mail: sakai@asrc.cestm.albany.edu

TABLE 1. Energy budget closure for several experiments.

Study	Energy budget closure $(H + LE)/A$	Instrumentation	Methods for mean removal
Pattey et al. (1997)	0.91	KD[a], IRGA[b]	Block average 0.5 h
Baldocchi et al. (1997)	0.94	ATI[c], open-path IR analyzer	400-s recursive filter and 0.5-h flux calculation
Goulden et al. (1997)	0.81	ATI[c], IRGA[b]	Linear fit detrend 0.5-h flux
Blanken et al. (1997)	0.87	KD[a], IRGA[b]	Block average 0.5 h
Jarvis et al. (1997)	0.97	SG[d], IRGA[b]	200-s recursive filter 0.5-h period
Lafleur et al. (1997)	0.75–0.81	CA27[e], KH20[f]	Block average 0.5 h (daily averaged)
McCaughey et al. (1997)	0.85–0.95	CA27[e], KH20[f]	Block average 0.5 h (daily averaged)
Blanken et al. (1997)	0.98	KD[a], IRGA[b]	Block average 0.5 h (daily averaged)
Lee and Black (1993)	0.82	CA27[c], KH20[f]	Block average 0.5 h (daily averaged)
Fitzjarrald and Moore (1994)	0.90	ATI[c], KH20[f]	240-s running-mean average, 0.5-h period
Barr et al. (1994)	0.91	KD[a], LH[g]	Block average 0.5-h average

[a] KD-310: 3D Kaiji–Denki (DAT310).
[b] IRGA: Infrared gas analyzer (LI-6262), LI-COR, Inc.
[c] ATI: 3D sonic anemometer, Applied Technologies, Inc., model SWS-211.
[d] SG: 3D Solent Gill sonic anemometer, Gill, Inc.
[e] CA27: ID sonic anemometer model CA20, Campbell Scientific, Inc.
[f] KH20: krypton hygrometer, model KH20, Campbell Scientific, Inc.
[g] OH: Lyman-alpha hygrometer.

in the atmosphere into sensible heat flux H, latent heat flux LE, the energy stored in canopy air and tree boles St, and the sum of sensible and latent heat advected Adv. The imbalance in the observed energy balance usually changes sign from night to day. For this reason, evaluating the eddy covariance methods by using daily averages of the energy balance is misleading; daytime errors usually partially cancel nocturnal errors of the opposite sign. We consider the convective case separately here.

Other eddy flux measurements made over forests also have been called into question. There is a mismatch between relatively small nocturnal carbon dioxide (CO_2) flux and more ''ecologically correct'' chamber measurements and model predictions (Baldocchi et al. 2000). Reconciling the disparate observations has prompted researchers to propose solutions for the systematic underestimation in eddy fluxes. Lee (1998) argued that the CO_2 budget must include terms resulting from mean vertical advection, possibly provoked by nocturnal drainage flow (Lee 1998; Baldocchi et al. 1997), but this argument has been disputed (Finnigan 1999). The actual presence of the drainage flows at tower flux sites has not yet been convincingly documented. The required subcanopy horizontal CO_2 flux divergence in the subcanopy has received even less attention. Blanken et al. (1998) and Goulden et al. (1996) argued that turbulent fluxes are underestimated under low values of friction velocity u_* (day or night). They propose that when there is inadequate mixing, the stationarity and zero-airmass-flow assumptions of the eddy covariance method are not valid. For daytime conditions, Mahrt et al. (1994) proposed that motions with horizontal scales larger than 10 km could contribute significantly to the turbulent flux measurement. The presence of local circulations such as the lake breeze is thought to produce motions on this scale (e.g., Sun et al. 1997). Mahrt et al. (1994), noting that lower fluxes are observed under light wind-speed days, proposed that daytime quasi-stationary eddies form over the tower—motions that could not be detected by the tower-based instruments. We do not discount the possibility that mean vertical advection, nocturnal drainage flows, or stationary eddies may influence flux measurement. However, it seems unlikely that *all* towers are sited incorrectly in the *same* way.

Low-frequency turbulent signals, probably associated with the convective boundary layer (CBL)–scale eddies, may be important. The flux-variable correlation coefficients for the low-frequency bandpassed signals for a sample case (Fig. 1) are within 8%–12% of the flux calculated using a 30-min centered running-mean removal. The ''EUROFLUX'' methodology suggests that a 3.3–16.67-min running mean should be applied to perform the mean removal (Aubinet et al. 2000). The choice of averaging period should not be arbitrary. Although a 16.67-min period can be used to detect most of the large oscillations in this case, a 3.3-min running mean would effectively filter the PBL contribution. Though an appreciable fraction of the variance comes from eddies in the inertial subrange, this frequency band is not as important for scalar covariances. In convective conditions, scalar cospectra in this band drop off with a steep $-7/3$ power law (Wyngaard and Coté 1972). As a consequence, although both the spectra and cospectra have low-frequency contributions, such contributions have more impact on the cospectra and the fluxes.

Kaimal et al. (1972) presented dimensionless cospectra for the scalar fluxes in the surface layer (SL) over nearly flat terrain. Their analytical forms continue to be cited widely to this day. These expressions, which de-

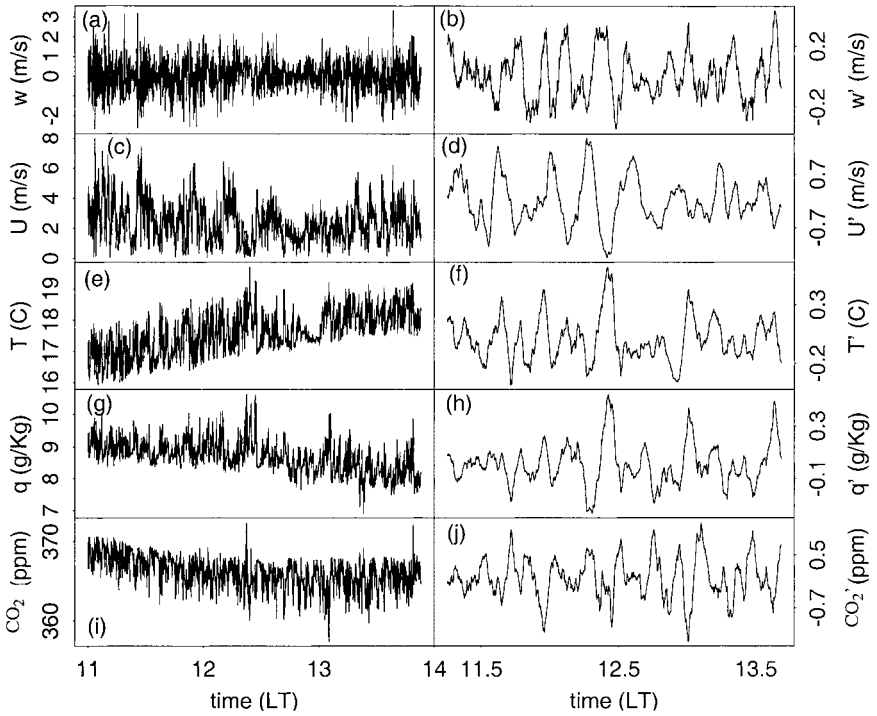

FIG. 1. (left) One-hertz time series of (a) vertical wind speed w; (c) horizontal wind speed U; (e) sonic temperature T; (f) specific humidity q; and (h) carbon dioxide concentration CO_2, measured on 29 Aug 1997 at Harvard Forest. (right) Smoothed data that result from passing a running-mean bandpass filter (4–30 min) over the data on the left. The correlation coefficients r_{wx} for a 30-min running mean of r_{wU}, r_{wT}, r_{wq}, and r_{wCO2} are −0.37, 0.52, 0.33, and −0.34, respectively. For the bandpass variables, the correlation coefficients are −0.26, 0.45, 0.42, and −0.49.

pend only on stability z/L (where z is the height above the surface and L is Monin–Obukhov length), refer to the inertial sublayer (IL), the uppermost sublayer in the SL. Sampling limitations lead to there being considerable scatter in cospectra at low frequencies—Kaimal et al. (1972) presented only a band of values for convective conditions. The RSL is that part of the SL in which the effects of the size of roughness elements are important to the turbulence. It is difficult to find real-world signals that are stationary for sufficient time that the low-frequency contributions can be found using fixed-point sensors. KF94 (p. 104) noted: ''Cospectra of w and θ [*vertical velocity and temperature in the RSL*] have . . . been presented on too few occasions to draw any general conclusions.'' Few new results have been reported since then. Large, carefully selected datasets must be composited to arrive at ''smooth'' results.

A potentially important lower-frequency contribution to eddy fluxes results from the actions of CBL eddies. These eddies, comparable in scale to the thickness z_i of the layer, are advected past a tower by the mean horizontal wind. The ideal averaging period should include an appreciable number (6–10) of the characteristic CBL timescales (z_i/w_*), where w_* is free-convection velocity scale). We assess the importance of large eddies in the flux calculation by determining a cospectral similarity expression for the RSL. We show (sections 3b,c below) that spectral and cospectral shapes for the RSL differ significantly from the ones found in the IL (e.g., KF94, p. 97). We assemble the largest dataset of observations to be used for this purpose to date. To approximate stationary conditions, we consider only periods in early afternoon, when surface fluxes and the mixed-layer thickness are not changing rapidly. The choice of suitable mean removal method can be crucial for capturing the whole eddy spectrum passing the tower. The turbulent fluxes are estimated by finding the running-mean period that can detect those eddies (section 3b). Using these flux values closes the observational energy balance in the afternoon for our cases. In section 3d, we compare fluxes calculated using several standard methods of determining the mean removal. RSL cospectral forms are discussed in section 3c. In the conclusions, we note how undersampled daytime flux also can represent an important bias in current CO_2 uptake estimates based on eddy flux measurements.

2. Methodology

a. Site descriptions and instruments deployed

A detailed description of the Harvard Forest (HF; 42.54°N, 72.18°W) experimental site, predominantly

TABLE 2. Description of the canopies: d is the displacement height (Sakai 2000), z_r is the level of the eddy covariance system, z_0 is the RSL, $\overline{w'T'}$ is the sensible-heat flux, and Cd is the drag coefficient. All those parameters were calculated using noon-period data. The CBL parameters at HF were estimated using Albany, NY, radiosondes (close to HF) and NOJP. The CBL height z_i was provided by J. M. Freedmann (1999, personal communication). Here, T_{CBL} is the CBL timescale that is calculated from the ratio between z_i and the free-convection wind speed w_*.

Experiment	BOREAS–NOJP	HF	
Location	Thompson, MB, Canada (55.92°N, 98.58°W)	Petersham, MA (42.54°N, 72.18°W)	
Dominant species	Old jack pine	Red maple and oak	
Canopy state	Evergreen	Foliated	Leafless
Plant area index	1.6 (Chen et al. 1997)	5	1.0
Canopy height (m)	8	23	23
z_r (m)	31.5	30.0	30.0
d (m)	5.5	17.8	13.8
z_0 (m)	0.8	1.2	2.4
$w'T'$ (°C m s^{-1})	0.196	0.102	0.0889
Cd	0.015	0.019	0.031
z_i (m)	969	698	837
w_* (m s^{-1})	2.13	1.32	1.14
T_{CBL} (min)	7.6	8.8	12.2

oak and maple, has been reported previously (Wofsy et al. 1993; Moore et al. 1996). The boreal forest site consists of jack pine and is part of the Boreal Ecosystem Study [BOREAS; Northern Study Area–Old Jack Pine (NOJP) site, 55.92°N, 98.58°W]. It is located near Thompson, Manitoba, Canada. A more detailed description of this dataset can be found in Moore et al. (2000). These two forests have very different characteristics (Table 2).

A three-dimensional sonic anemometer (model SWS; Applied Technologies, Inc.), measured wind speed and temperature signals at 10 Hz at the top of each tower (30 m). Water vapor (H_2O) and CO_2 signals at the same rate were observed using an LI6262 CO_2/H_2O instrument from LI-COR, Inc. The inlet was positioned at tower top, and the air was pumped to the sensor at ground level, with a travel time of about 4 s. The separation distance between the sonic anemometer and the inlet is 0.5 m.

In both experiments, net radiation was calculated from the sum of the upward and downward global solar and terrestrial radiative fluxes observed at 27 m. To measure solar radiation, upward- and downward-facing Kipp and Zonen, Inc., radiometers were deployed (model CM11 at HF; model CM14 at NOJP). Photosynthetically active radiation (PAR) sensors (LI-COR model LI190SA) measured the upward and downward global visible radiation (400–700 nm). The upwelling and downwelling terrestrial radiation were measured using Eppley Laboratory, Inc., pyrgeometers (model PIR) at HF and a Kipp and Zonen (model CG-2) at NOJP.

Radiation and Energy Balance Systems, Inc., soil heat flux plates (models HFT-1 and HFT-3.1) were installed at 3.8 and 5.0 cm below the organic layer at NOJP and HF respectively. Soil temperature probes (Campbell Scientific, Inc., model M107) were installed at three vertical levels (0.025, 0.075, and 0.20 m below the surface). At NOJP, the forest floor is covered by lichen whose depth is about 5.0 cm. At HF, the organic layer is about 2.5 cm. To evaluate the soil heat flux at the interface of the organic layer, an extrapolation using the soil temperature profile and the observed soil heat flux was done.

The canopy storage was calculated according to Moore and Fisch (1986), using a wood heat capacity of 1.52×10^6 J m^{-3} K^{-1} (Oke, 1987, p. 259). During the 1996 campaign, model M107 temperature probes were placed at three levels in a ''typical'' old jack pine trunk at NOJP site. The basal area is 16.9 m^2 ha^{-1} (Gower et al. 1997). During the noon period, canopy storage values obtained during the 1996 campaign have median values of 8.9 ± 3.4 W m^{-2}, with a maximum value smaller than 25 W m^{-2} in NOJP.

Because no trunk temperatures are available for HF, heat storage in the wood was estimated using the canopy-layer air temperature with a typical wood heat capacity. See Sakai (2000) for details. The basal area at HF, according to a 1986–1993 survey, is about 36.4 m^2 ha^{-1} (http://www.lternet.edu/hfr). At the noon period in HF, canopy storage evaluated from the air temperature profile is 27 ± 13 and 17 ± 25 W m^{-2} during the foliated and leafless periods, respectively. This magnitude is within the range of values found in another deciduous forest (Barr et al. 1994).

b. Turbulent flux data

Three-hour periods centered on local noon were selected. At this time of day, the CBL height is typically about constant (Blackadar 1979). Fluxes during this period contribute on average about 52%, 42%, and 30% of the daytime turbulent fluxes for heat, water vapor, and momentum, respectively. Data analyzed were originally sampled at 10 Hz; 1-Hz average data were used for this analysis. Candidate days were eliminated if visual inspection of the data indicated that the number of spikes in the 1-Hz average data exceeded 12. If only a few spikes were found, these points were replaced by a value interpolated linearly between adjacent points. Spike definition thresholds for horizontal and vertical wind speeds, for example, are 5 and 2.5 m s^{-1}, respectively. No other selection was made (e.g., for clear or cloudy days or specific wind directions). For HF, 83 days from August to December of 1997 were considered (43 days for the foliated period, 24 days for the leafless period, and 16 days for the transition period). Most of the wind was coming from the direction that was not being obstructed by the tower (about 75% of the study cases). At NOJP, 21 days during August and September of 1994 were used. In BOREAS, the sonic anemometer was rotated to point against the flow once a day in the morning. The Webb correction was performed for the CO_2 and water vapor fluxes (Webb et al. 1980), and three-dimensional rotation of the coordinates was ap-

plied to the wind components (McMillen 1988) using block-average values for each 3-h period. The rotation angle between the horizontal and the vertical wind speed ranged from $-3.8°$ to $+3.5°$. This corresponded to relative differences of about 5% and 2% for scalars and momentum fluxes respectively. A spectral correction for damping of the specific humidity q and CO_2 signals by tube attenuation was made by assuming that the w–T and w–q or w–CO_2 phase angles (w is vertical wind speed; T is sonic temperature) are identical in the inertial subrange (Sakai 2000). The lowest frequency at which the correction is applied was derived from a tube-attenuation formula given by Leuning and Moncrieff (1990). This correction gives a median increase of 4% and 5% for H_2O and CO_2 fluxes, respectively.

Finding the perturbation time series involves removing mean quantities, which is equivalent to filtering. Expressions for transfer functions for the centered running-mean, block-average, and linear-trend methods to estimate mean quantities are given in the appendix. Massman (2000), Rannik and Vesala (1999), and Sakai (2000) present more details.

3. Data analysis and discussion

a. Stationarity

For a stationary time series, statistical moments for a long period should be equivalent to those found using shorter periods. Because periods longer than the traditional 20–30-min periods are used in this study, we assess the stationarity of elements in the resulting averages. Three-hour periods for the horizontal and the vertical wind speed were divided into six nonoverlapping segments of 30 min each (t_{div}) during the midday period (t_{all}). Thirty-minute periods, longer than those typically used (e.g., Foken and Wichura 1996), are employed, in recognition of the long-period oscillations in the time series (Fig. 1). The mean (avg), standard deviation (std dev), skewness (skw), and kurtosis (krt) are calculated for t_{all} and for each t_{div}. Then, a regression line is fitted between the moments from t_{all} and its respective set of t_{div}. The running mean period used was 30 min, and it was applied before the period was divided.

A slope close to 1 and an intercept close to 0 in Table 3 indicate that there is little average difference between each individual segment (t_{div}) and the whole interval (t_{all}), and turbulence properties can be considered to be approximately stationary. Among the statistical parameters, skw shows the poorest results, principally for the block average and for the linear fit. Using the $t_{0.001}$ value as the error for the skw slope values, the relative error is 16.9%, 16.4%, and 12.6% for the block average, linear trend, and running mean, respectively. Lower residual standard errors in the liner regression (rse) for the running-mean filter suggest the turbulence appears more stationary when this procedure is used, indicating that diurnal variation is removed more effectively. Results for w are similar to those for the horizontal wind speed.

TABLE 3. Stationarity statistics for the horizontal wind speed for HF. Here, the $t_{0.001}$ column corresponds to the slope ranges with a 99.9% confidence using t distribution. For instance, 99.9% of the skw slope values are within 0.779 ± 0.132 for the block averages. Here, r^2 is the variance.

Conditioning	Moment	Intercept	Slope	r^2	$T_{0.001}$	Rse
Block average	Avg	0.016	0.997	0.87	0.057	0.36
	Std dev	−0.0076	0.969	0.89	0.050	0.38
	Skw	−0.053	0.780	0.43	0.13	0.33
	Krt	−0.58	0.908	0.88	0.049	2.2
Linear fit	Avg	0.016	0.997	0.87	0.057	0.36
	Std dev	−0.086	0.964	0.90	0.048	0.36
	Skw	−0.037	0.770	0.44	0.13	0.30
	Krt	−0.58	0.901	0.89	0.046	2.0
Running mean	Avg	0.0086	0.998	0.94	0.038	0.23
	Std dev	−0.0018	1.002	0.94	0.037	0.27
	Skw	0.0041	0.970	0.58	0.12	0.25
	Krt	−0.075	0.994	0.94	0.037	1.53

b. Low-frequency contributions to eddy fluxes

If a running-mean bandpass filter is applied to the sample time series (Fig. 1), the presence of well-correlated 4–30-min oscillations in all signals is apparent (Figs. 1b,d,f,h,j). The period of these quasi-periodic oscillations is longer than that of the intermittent, nonperiodic coherent structures observed in the RSL above forests (less than 4 min; Lu and Fitzjarrald 1994). The periods of the organized structures (Fig. 1, right) are similar to the CBL timescale (z_i/w_*; see Table 2). This timescale is smaller for the NOJP data than for HF, because larger sensible heat fluxes [and the corresponding free-convection velocity scale $w_* = (g\overline{w'T'}/T)^{1/3}$, where g is gravitational acceleration and primes indicate perturbations] were encountered at NOJP.

When using centered running means to calculate the deviations, it is well known that the mean of the deviations need not necessarily vanish (e.g., KF 94, p. 266). For the datasets used here, this is not a problem. The largest contribution from the mean product (the zero harmonic in the cospectrum) is less than 0.1% of the total flux when the mean is found using a 30-min running mean. Using the 1-Hz data also poses little difficulty: frequencies higher than 0.5 Hz contribute on average less than 1% of the total flux.

The variance reported depends on the filter period used to define the mean (Fig. 2). Here, U (horizontal wind speed), T, q, and CO_2 variances increase steadily up to the longest running-mean period (60 min). However, the w variance becomes independent for periods exceeding 30 min. In contrast, the normalized flux curves (Figs. 2c,d) flatten when a 30-min-or-longer running-mean filter is applied. For the entire dataset considered here (HF and BOREAS), 4–30-min-period oscillations contribute about 17% to the total turbulent

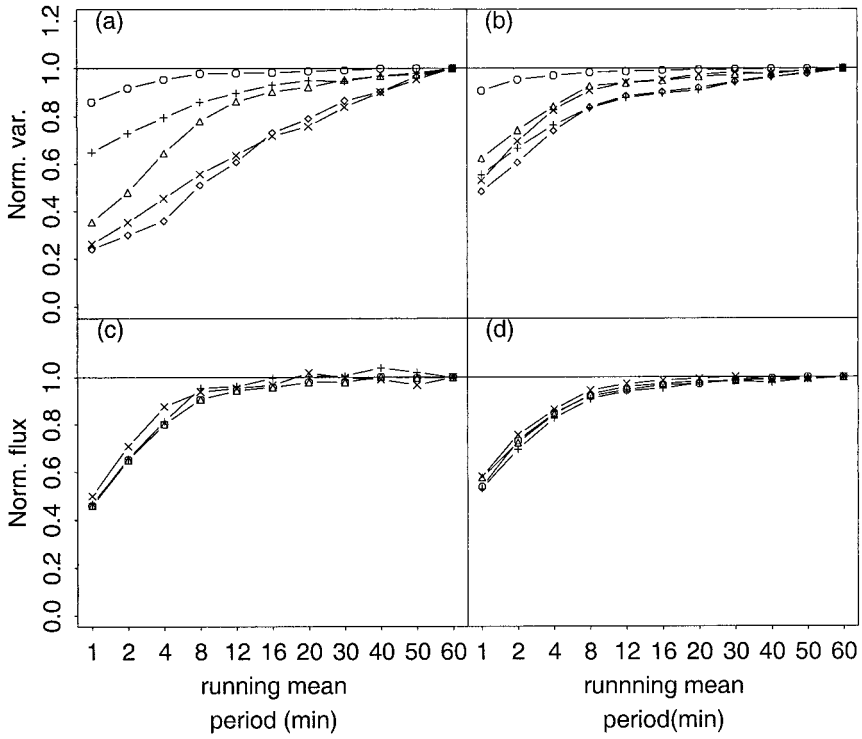

FIG. 2. (top) Normalized variance vs running-mean filter period for w (circles), U (triangles), T (pluses), q (crosses), and CO_2 (diamonds) for (a) NOJP and (b) HF data. The variance is normalized by the 60-min high-pass filter variance. (bottom) Normalized covariance vs running-mean filter period for $\overline{w'U'}$ (dots), $\overline{w'T'}$ (triangles), $\overline{w'q'}$ (pluses), and $\overline{w'CO_2'}$ (crosses) for (c) NOJP and (d) HF data. The covariance is normalized by the 60-min high-pass filter variance.

flux. This result is highly dependent on mean wind speed (see below).

We define an *averaging-period wind run* to be the running-mean period multiplied by the average wind speed. When translated into wind run, the fluxes stabilize at 6–8 km (Fig. 3). This result is consistent with those from earlier case studies based on aircraft measurements. Mahrt (1998) noted: ''For flight levels even as low as 30 m, significant transport may occur on scales larger than 5 or 10 km. . . .'' For aircraft flying at low altitude (30 m) in BOREAS, the contribution of horizontal scales longer than 3.5 km is about 10% for sensible heat flux (Desjardin et al. 1997).

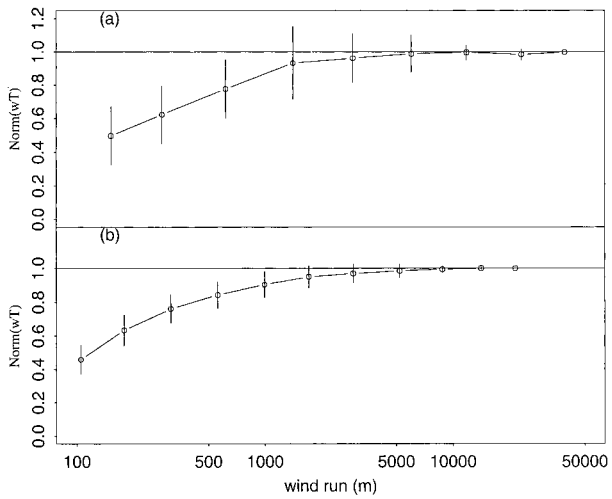

FIG. 3. Wind-run plot for (a) NOJP and (b) HF. Vertical segments represent the standard deviations for the days analyzed.

For the NOJP experiments, 80% of the flux originates from a source area, or footprint area, at an upwind distance of about 700 m (Kaharabata et al. 1997), about the same value as the averaging-period wind run required to calculate 83% of the flux (Fig. 3a). Similar results are found in other footprint studies (Schuepp et al. 1990; Horst and Weil 1991). However, the footprint radius is a different concept from our averaging-period wind run. When calculating the footprint, one associates the turbulent fluxes with a source region located upwind of a tower-based measurement and calculates vertical dispersion based on Monin–Obukhov similarity expression for standard deviation of the vertical wind speed σ_w (Horst and Weil 1994; Baldocchi 1997). Thus, as it is often applied, the footprint accounts only for the SL mixing processes. Moreover, the footprint radius tends to *shrink* in convective conditions.

The cospectral consequences of including the longer-period oscillations are illustrated in Fig. 4 for momen-

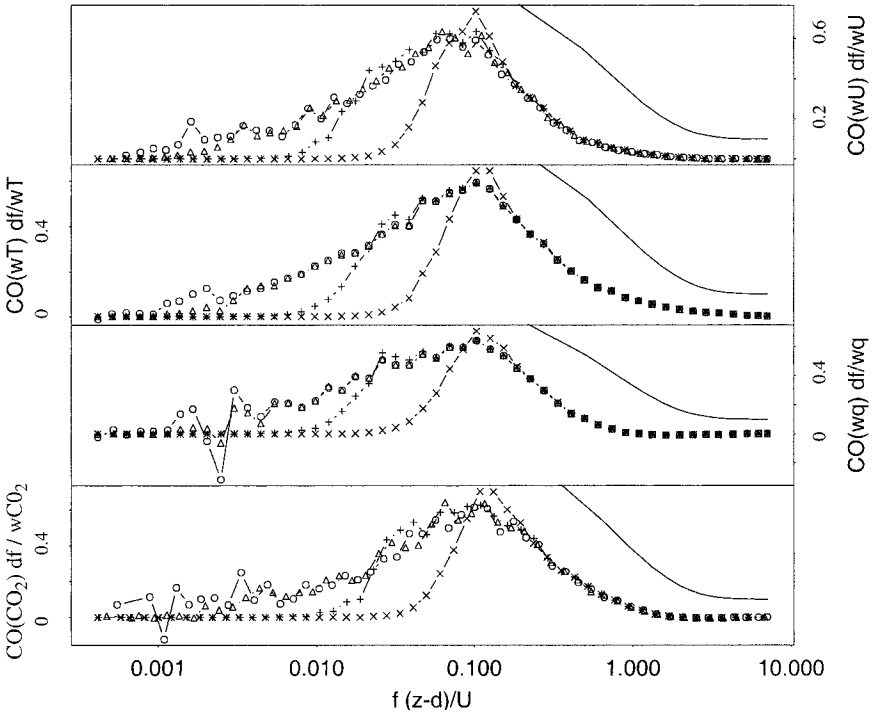

FIG. 4. Normalized cospectra for (top) $\overline{w'U'}$, (second from top) $\overline{w'T'}$, (third from top) $\overline{w'q'}$, and (bottom) $\overline{w'CO_2'}$ Crosses represent the flux using a 1-min running-mean filter, pluses are for a 4-min running-mean filter, triangles are for a 30-min running-mean filter, and circles are for a 60-min running-mean filter for HF. Solid curved line represents the $-7/3$ power law.

tum, heat, water vapor, and CO_2 fluxes. We define the *excess flux* as $(F_{30} - F_4)/F_4$, where F indicates the turbulent flux and the subscript represents the running-mean filter length in minutes. The excess flux depends on the stability parameter [$\zeta = -(z - d)/L$; Fig. 5a], where d is the displacement height calculated taking into account the vertical-profile canopy area density (Sakai 2000). In the free-convection regime ($\zeta > 0.5$; e.g., Garstang and Fitzjarrald 1999, p. 117), there is more excess flux. With the current two datasets, we cannot distinguish ζ and z_i/L functionality, given that z_i is about the same size in both situations. The excess flux is better seen to be a simple function of wind speed alone (Fig. 5b). The fitted curves in Fig. 5b are given by $wT_{\text{exc}} = a_0 + a_1/U$, where wT_{exc} is excess flux, and a_0 and a_1 are the slope and intercept of the linear regression of wT_{exc} and $1/U$ (Table 4).

c. *Cospectral similarity in the RSL—Empirical functions*

Normalized cospectral curves for all quantities considered exhibit similarity properties, collapsing to a single curve in a dimensionless frequency domain for each site (Fig. 6). Wyngaard and Coté (1972) proposed that, at high frequencies, the cospectrum follows a 7/3 power decay. The only cospectra that do not exhibit this form are those of the water vapor and the carbon dioxide signals, and this results from attenuation of high frequencies in the sampling tube. For both foliated and leafless conditions at HF, there is a common cospectral shape, illustrated by the w–T cospectrum in Fig. 7. In the RSL, the cospectra are more peaked than the IL ones, a consequence of more intense mixing in the RSL. NOJP spectra have a shape more similar to those reported for the Kansas and Minnesota experiments (Fig. 7; Kaimal et al. 1972; Kaimal 1978). The remaining functionality for convective conditions depends on the position of the eddy covariance sensor within the RSL. The closer the instruments are to the IL, the more similar are the cospectra shapes to the IL forms. Thus, our results indicate that there is cospectral similarity in the RSL and that the relevant height variable in this layer is $(z - d)/(h - d)$, where h is the canopy height. Sakai (2000) found that the depth of the RSL can also be defined as the crossover point from negative to positive values in the skw profile when plotted versus dimensionless height [$(z - d)/(h - d)$].

Over flat surfaces, the cospectrum CO(wU) is more peaked than is CO(wT), but the two are nearly identical in the RSL. The difference between CO(wU) and CO(wT) at HF is much smaller than that observed for Kansas and NOJP. Enhanced mixing in the RSL tends to ''homogenize'' the cospectra of the turbulent fluxes at high frequencies (dimensionless frequency $f' > 0.1$). At low frequencies, the cospectra shapes are similar to

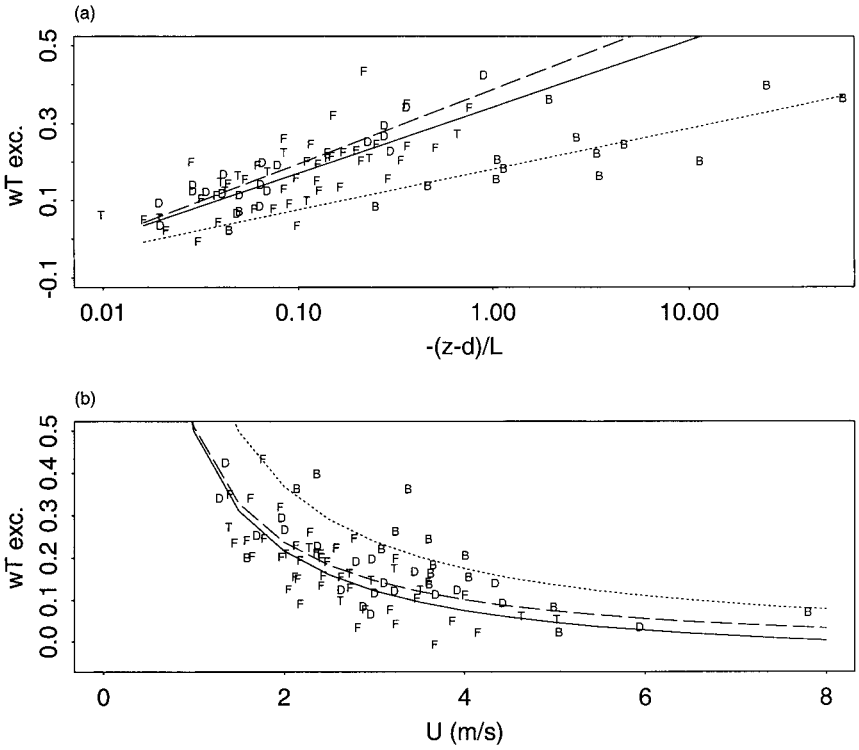

FIG. 5. (a) Plot of excess of flux (see text) vs stability parameter for HF and NOJP dataset. Here, F represents the HF-foliated period, D stands for HF-leafless period, T is for the transition period, and B is the NOJP dataset. Solid line is the fitted line for HF foliated; dashed line is for HF leafless; dotted line is for NOJP. (b) Same as (a), but for the wind speed: solid line represents the fitted line to the inverse of U during HF-foliated period; dashed line is for the HF-leafless period; the dotted line is for NOJP (see Table 5).

the ones found in the IL. These RSL cospectral shapes are consistent with those found in case studies of very limited duration for near-neutral conditions for another deciduous forest (Anderson et al. 1986).

''True'' empirical similarity forms for the spectra and cospectra are given by the composites of data (Fig. 8). To aid in making a transfer-function flux correction scheme, we seek analytical forms for the RSL cospectra. Curves that satisfy the normalization and asymptotic frequency constraints can be fitted to the data. An analytical, normalized empirical cospectral density function is given by

$$\frac{f\,\mathrm{CO}(wx)}{\overline{w'x'}} = \frac{\beta_1 f'}{1 + (\beta_2 f')^{7/3}}, \qquad (2)$$

where f' is the dimensionless frequency [$f' = (z - d)f/U$]. The results are presented in Table 5, and the details are given in Sakai (2000). Massman (2000) performed a similar analysis, using the Kaimal et al. (1972) cospectra. The standard deviations for the parameters β_1 and β_2 (Table 5) indicate that there are not many differences among the fitted cospectral curves. Moreover, the use of a single form for all cospectra yields only a relative increase of 10% in rse for the NOJP CO(w–CO_2) curve. Thus, the error introduced is small.

TABLE 4. Parameters for fitted line $1/U$ and excess flux presented in Fig. 5b. Here, a_0 is the intercept and a_1 is the slope.

	$z - d$ (m)	a_0	a_1	r^2
NOJP	26	−0.020 ± 0.010	0.777 ± 0.054	0.7
HF (foliated)	12.2	−0.071 ± 0.042	0.579 ± 0.095	0.5
HF (nonfoliated)	16.2	−0.036 ± 0.027	0.551 ± 0.065	0.8

Blanken et al. (1998) and Jork et al. (1998) argued that turbulent fluxes are underestimated under low mixing conditions, that is, when u_* is small. This is supposed to be because mass flow and advective effects are unaccounted for in the eddy covariance. We agree that important advective effects need to be considered, but our interpretation is different. To us, an additional important explanation for missing daytime flux is inadequate sampling of the turbulent long-period fluctuations under light-wind conditions in daytime. We arrive at conclusions similar to those of the previous authors because there is a high correlation between U and u_*.

Using the transfer function [appendix, Eqs. (A3) and (A4)] for a given running-mean averaging period and the modeled cospectrum, we examine the effects of different mean definitions (Fig. 4). This procedure is very

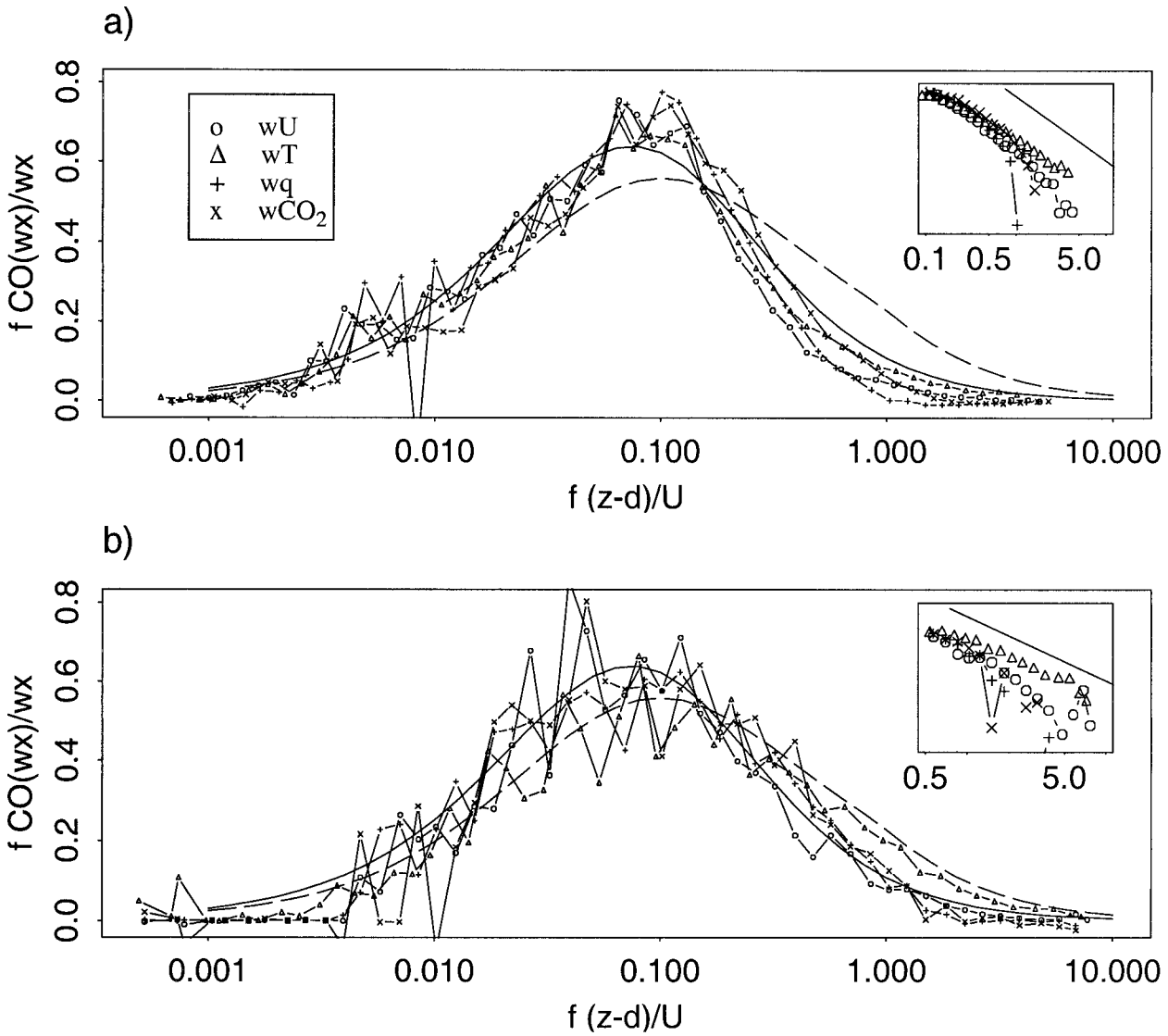

FIG. 6. Cospectra from (a) HF-foliated and (b) NOJP experiments; circles, triangles, pluses, and crosses correspond to CO(wU) (43 runs for HF and 21 for NOJP), CO(wT) (43 runs for HF and 21 for NOJP), CO(wq) (35 runs for HF and 16 for NOJP), and CO($w\mathrm{CO}_2$) (33 runs for HF and 14 for NOJP), respectively. The solid line is the CO(wU), and the dashed line is the CO(wT) for a flat surface (Kaimal et al. 1972). The inset is the cospectra log–log plot for high frequencies; the straight line represents the $-7/3$ power law.

similar to that used in Kristensen and Fitzjarrald (1984), though in that study the authors focused only on the high-frequency regions.

The flux correction is based on the following formula:

$$\overline{w'x'}_{\mathrm{corr}} = \frac{\int \mathrm{CO}(wx)\, df'}{\int (|1 - H(f')|)^2 \mathrm{CO}(wx)\, df'} \overline{w'x'}, \quad (3)$$

where CO(wx) is the normalized cospectral form given in Table 5, $\overline{w'x'}$ and $\overline{w'x'}_{\mathrm{corr}}$ are the calculated and corrected fluxes respectively, and $H(f')$ is the transfer function for the mean removal (low-pass filter). Note that if a high-pass filter is used to estimate the deviations, then $[|H(f')|^2]$ has to be used instead of $\{|1 - [H(f')|]^2\}$ in the denominator of Eq. (3). To make a similar correction for other averaging procedures, one finds the transfer function of the mean removal and applies this to the similarity expression for the normalized cospectrum.

d. Results of using different mean-removal methods

In this section we present comparisons between the fluxes obtained using the running-mean filter and those found using other traditional methods of mean removal, including the simple average and a linear trend. The 3-

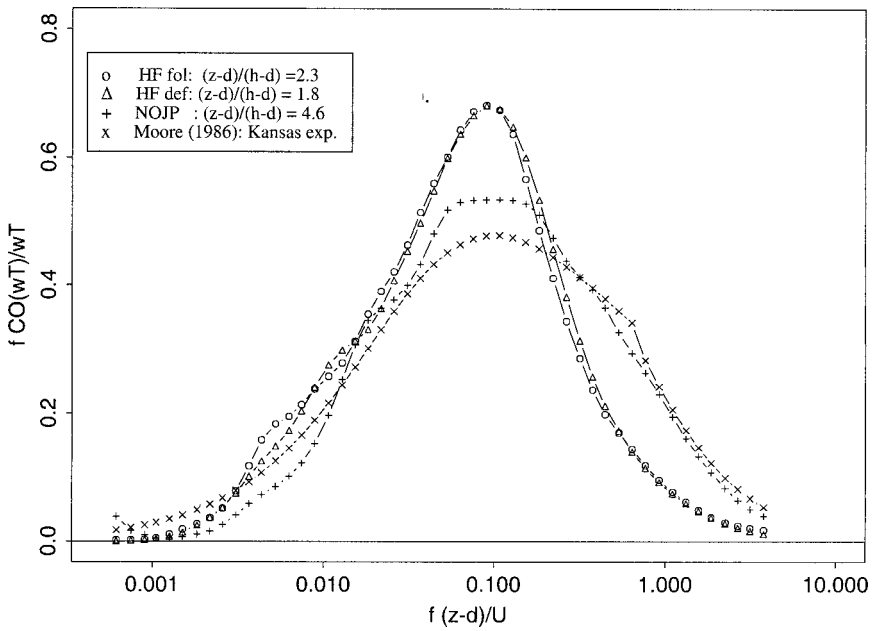

FIG. 7. Normalized smoothed $\overline{w'T'}$ cospectra for a foliated (HF fol) and leafless (HF def) deciduous forest, boreal forest (NOJP), and over a flat surface (Moore 1986).

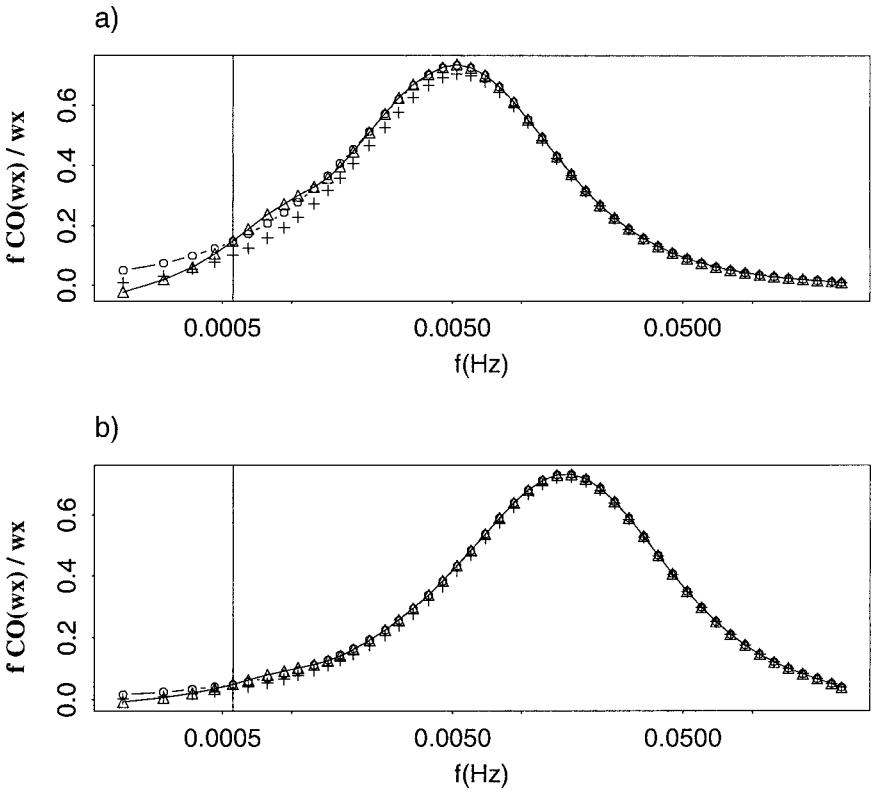

FIG. 8. Modeled cospectra for (a) $U = 1$ and (b) $U = 5$ m s^{-1}. Solid line is the modeled cospectra without the filter function. Circles, triangles, and crosses correspond to the cospectra value times the transfer function of the running mean, blocking average, and linear trend, respectively.

TABLE 5. Parameters for the cospectral curves in Fig. 6.

Site	Cospectrum	β_1	β_2	Rse
HF foliated	CO(wT)	7.61 ± 1.3	11.5 ± 1.8	0.0043
$z - d$ = 12.2 m	CO(wU)	8.51 ± 1.7	12.4 ± 2.4	0.0044
	CO(wq)	7.92 ± 1.3	11.4 ± 1.8	0.0064
	CO($w\mathrm{CO}_2$)	6.71 ± 1.5	9.7 ± 1.5	0.0039
HF leafless	CO(wT)	6.83 ± 1.2	10.2 ± 2.0	0.0043
($z - d$ = 16.2 m	CO(wU)	8.07 ± 2.5	11.5 ± 3.6	0.0034
	CO(wq)	7.81 ± 1.2	11.1 ± 2.0	0.0077
	CO($w\mathrm{CO}_2$)	5.71 ± 1.3	8.7 ± 2.0	0.087
NOJP	CO(wT)	4.78 ± 2.4	8.3 ± 2.1	0.0086
$z - d$ = 26.0 m	CO(wU)	8.09 ± 2.3	12.2 ± 3.9	0.0076
	CO(wq)	6.67 ± 1.9	10.1 ± 2.2	0.0082
	CO($w\mathrm{CO}_2$)	7.29 ± 1.5	10.4 ± 2.1	0.010
All curves		8.02 ± 2.5	10.7 ± 3.7	0.0073

h periods were divided into six 30-min segments. Then, the deviations were calculated in each segment and were compared with the value obtained using the 30-min running-mean filter. The resulting cospectra (Fig. 9) do not approach zero at low frequency, indicating that 30-min segments cannot resolve the whole cospectrum. To find the form of the RSL cospectrum, one must take an average period of 2- or 3-h length, which is considerably longer than the usual 20–30-min periods.

There is good agreement among fluxes calculated using the block average, the linear detrending technique, and the 30-min centered running-mean removals. For the whole period, the block average gives the highest value and the running mean gives the lowest. The contribution of the lowest frequency to the cospectra indicates that the averaging procedure is not properly removing the diurnal variation of the signals. This amounts to flux enhancements of only 3.2% and 0.1% from the total fluxes in the block average and the linear fit, respectively. The diurnal tendency that survives the blocking average leads to extra fluxes ranging from -8.5 to 30.1 W m^{-2} with an average of 4.1 W m^{-2} for the foliated period in HF. This effect can offset the effect of poor sampling of low-frequency eddies, depending on the sign of the slopes, and can lead the researcher to report enhanced fluxes—a case of getting the desired result for an inappropriate reason. Rannik and Vesala (1999) argued that linear trend removal is superior to using an autoregressive filter for determining fluxes. However, their analysis was performed using synthetic data for which the mean vertical velocity was specified to be zero. The relative merits of mean removal techniques may vary with the background environment. To apply a cospectral correction procedure for data originally taken with 0.5-h averages, some kind of filtering is superior to simple linear trend removal.

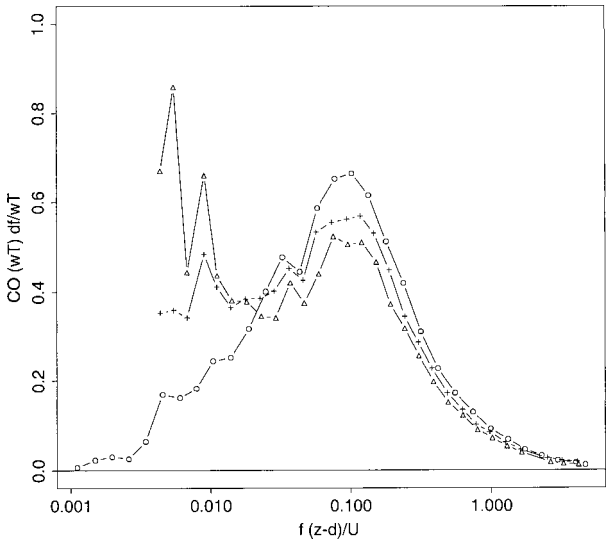

FIG. 9. Semilogarithmic plot of wT cospectra using different types of mean removal: 30-min running mean (circles), 30-min average (triangles), and linear trend removal (pluses).

e. Surface energy budget

Assessing the balance between the available energy and the sum of the sensible- and latent-heat flux and storage is one way to evaluate quality of the turbulent flux measurements. When a 4-min running-mean period is used to obtain the estimate the fluxes, (H + LE + St) versus [$A = (Q_* - G)$] slopes are about 0.81, 0.68, and 0.83 for HF foliated, HF leafless, and NOJP, respectively. If the fluxes are estimated using the 30-min running mean, calculating for 3-h periods (Fig. 10a), regression lines give slopes of 0.99, 0.76, and 0.98 for HF foliated, HF leafless, and NOJP, respectively.

At HF in leafless conditions, the energy budget does not close ($A > H$ + LE + St). One possible explanation is that the understory vegetation makes a sizable contribution to St, because the canopy is more open, and thus more net radiation is available at those levels. However, this may not be the only explanation for the HF-leafless results. The slope (0.756) in Fig. 10a for HF leafless suggests that other factors are contributing to

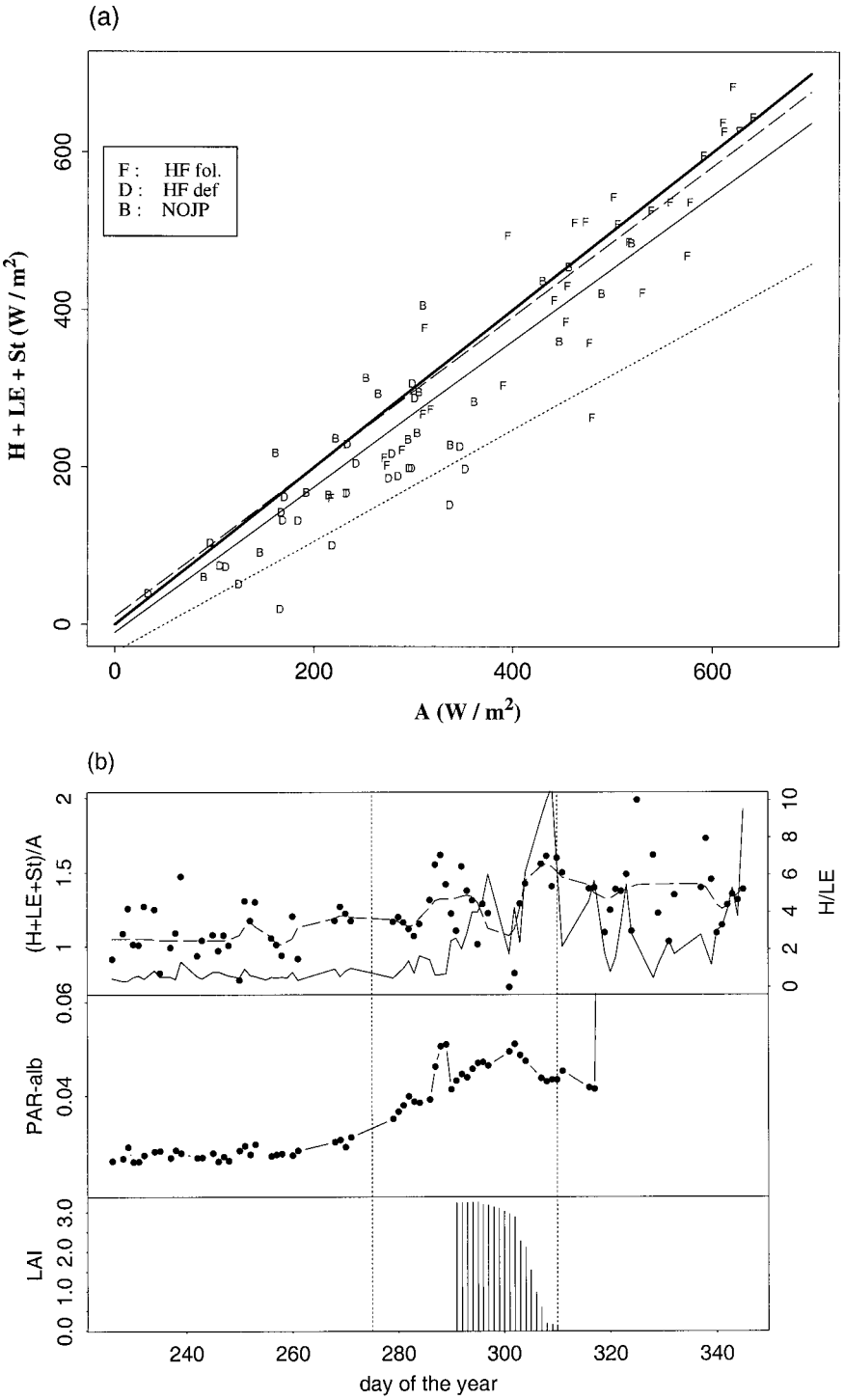

FIG. 10. (a) Scatterplot of the energy budget for HF and NOJP. Here, B corresponds to NOJP data, F corresponds to foliated period in HF, D stands for leafless period in HF. Dashed line represents the linear regression to HF foliated; dotted line represents the HF leafless period; solid-thin line represents the NOJP dataset; solid-thick line represents the 1:1 line. (b) (top) Time series for HF of the ratio (H + LE + St)/A represented by circles. The dashed line is a fitted curve for this ratio, and the solid line is the Bowen ratio (H/LE). (middle) Time series for HF of the PAR albedo (upward PAR over the downward PAR). (bottom) Leaf area index time series derived from the total solar radiation (Sakai et al. 1997). Vertical dashed lines represent the transition period that begins at the start of the leaf coloration and ends at the end of leaf fall.

the energy imbalance. This imbalance increases as the leaves change color (Fig. 10b). Leaf senescence at HF can be detected by changes of the albedo in the visible light (PAR albedo), and there is a substantial change in evaporation (Sakai et al. 1997). Thus, the increase of the residual in the energy budget is accompanied by an increase of the Bowen ratio during that period. One possibility is that the representativeness of the Q_* footprint area is reduced in the autumn. The autumn–winter field of view includes trunks and branches in proportions that may be less representative of the forest than would the summer field of view.

4. Summary and conclusions

This study illustrates the importance of relatively long-period fluctuations (4–30 min) to turbulent fluxes observed in the roughness sublayer over forests. Using data from two distinctive forests during noontime periods, methods to calculate turbulent fluxes from single point measurements have been studied. For the first time, we report normalized cospectral similarity functions to describe momentum and scalar fluxes in the RSL. In common practice, eddy fluxes are calculated at 0.5-h intervals. This method necessarily results in underestimation of the fluxes to a degree that depends on the choice of mean removal method, because this method fails to take into account the passage of low-frequency oscillations past the tower. Heat, moisture and carbon dioxide fluxes, for example, are probably underestimated in the daytime, principally under light-wind conditions.

Among the three methods considered to separate the mean flow from the perturbation—centered running mean, block average, and linear trend—we find that using the centered running mean results in a sufficiently stationary turbulent signal. Block average and linear detrending do not adequately remove the diurnal variation in this dataset. This result can be seen in the cospectral plots, for which the lowest frequencies do not go asymptotically to zero (Fig. 9). This feature makes a transfer-function correction difficult. The best running-mean filter found is 30 min applied to a 3-h period in midday.

Results suggest that air masses from as far as 7 km from the tower contribute significantly to the turbulent fluxes. Most of the turbulent fluxes (80%) are generated within 0.7–1 km downwind from the tower, a value consistent with that of footprint studies (Schuepp et al. 1990; Horst and Weil 1991; Kaharabata 1997). Based on the peak in the cospectrum, the dominant eddy size is on the order of 10% of the CBL size in convective conditions. A noticeable, but smaller, contribution to the turbulent fluxes, due to 4–30-min oscillations, which we associate with motions constrained by the CBL height, was observed in time series during noontime. This contribution accounts on average for a 17% increase of the turbulent fluxes. It is this contribution that needs to be accounted for to improve the energy balance closure during convective periods for NOJP and the foliated period in HF. We found, however, that this improvement inexplicably vanishes after the deciduous forest started to change colors in autumn season.

Cospectral curves in the RSL are more peaked than those in the inertial layer. If an eddy correlation flux observing system were to be located close to the IL, the cospectral shape of turbulent fluxes would be similar to the ones found by Kaimal et al. (1972). However, it is usually very difficult to build towers that are as much as four canopy heights above tall forests. Recent studies (Laubach and McNaughton 1998; Rannik and Vesala 1999; Massman 2000) used the Kaimal et al. (1972) or the KF94 cospectral fits appropriate for the IL to estimate spectral corrections and errors to the turbulent fluxes in the RSL. The use of IL cospectra curves for RSL cospectra leads to overestimates of turbulent fluxes for light-wind conditions, for instance.

It is clear that results for other scalar fluxes, most notably CO_2, are also being underestimated during convective conditions by many current tower observational systems. For instance, according to Goulden et al. (1996), the gross uptake of CO_2 at the Harvard Forest is about 11.7 Mg C ha^{-1} yr^{-1}. If we apply our correction to the noon period (1100–1400 LT), which accounts for about 42% of the total daytime flux, we find an increase of 7% in the total uptake. Making the daytime correction alone gives a revised gross uptake of 12.5 t C ha^{-1} yr^{-1}. We do not believe that such a large uptake estimate is valid. Rather, other errors, particularly at night, must be present. In the race to find why nocturnal fluxes are so ''small,'' the community has perhaps overlooked a daytime underestimate, which only exacerbates the problem. It would seem that there must be larger errors than previously understood in the nocturnal CO_2 flux estimate. Further investigation of nocturnal fluxes clearly is warranted.

Acknowledgments. During doctoral studies, RKS was supported by a NASA Office of Mission to Planet Earth Graduate Student Fellowship in Global Change Research (1995-GlobalCh00395). Measurements at Harvard Forest are supported by the U.S. Department of Energy's (DOE) National Institute for Global Environmental Change (NIGEC) through the NIGEC Northeast Regional Center at Harvard Forest (DOE Cooperative Agreement DE-FC03-ER61010) under Subcontract 901214 from Harvard University. Data from the ABLE 2A, 2B, 3A, 3B, and BOREAS projects were supported by NASA through Grants NAG-1583, NAG-1-692, NAG-1-847, NAG-11092, and NAG-52242, respectively, to the Research Foundation of the State University of New York.

APPENDIX

Filters for Means Definition

a. Centered running mean

Because of its simplicity and because no phase lag is introduced, the centered running mean was used to represent the mean flow:

$$\overline{x}_i = \frac{1}{N+1}\sum_{j=-N/2}^{N/2} x_j, \tag{A1}$$

where $\overline{x}$ is the filtered value, x_j is the raw signal, and $N + 1$ (odd number) is the length of the running mean. Another advantage in using running means is that the transfer function can be derived analytically. For a low-pass filter, its expression is given by (Hamming 1977, p. 22):

$$H(f) = \frac{\sin(N\pi f)}{(N)\sin(\pi f)}, \tag{A2}$$

where f is the frequency. Thus, if a 4-min filter is being used, for example, an oscillation at a frequency of 0.001 Hz will lose about 60% of its original signal.

b. Block average

One of the most traditional methods used to calculate the mean-flow term is to do the block average. In this technique, the average for a certain time interval is calculated, and then deviations are determined from that average.

For a block average, the transfer function for $\overline{x}$ is given by (Pasquill and Smith 1983):

$$H(f) = \frac{\sin(N\pi f)}{N\pi f}. \tag{A3}$$

c. Linear trend removal

Another method used to separate the flow is linear trend removal. One fits a straight line in a time interval, and the mean flow is represented by the fitted line. The Fourier transform of a straight line with intercept a and slope b within the window $t \in [-T/2, T/2]$ and zero elsewhere is:

$$F(f) = a\frac{\sin(\pi fT)}{\pi fT} + \frac{b}{2}\left[\frac{\cos(\pi fT)}{\pi f} - \frac{\sin(\pi fT)}{(\pi f)^2 T}\right]i, \tag{A4}$$

where $i \equiv \sqrt{-1}$, b is the slope, and a is the intercept from the line fitted for detrending. When the intercept a is not equal to 0, one can normalize Eq. (A4) by a, leading to the familiar ''top-hat'' window transfer function in the limit of no slope. Note that this transfer function has an imaginary part, indicating that a phase angle is introduced. When calculating cospectra, of course, one cannot assume that the slopes and intercepts for the two variables are the same. If a simple least squares fit is done (i.e., outliers are not removed arbitrarily or using some robust regression approach), then $a = (1/T)\int_{-T/2}^{T/2} u(t)\,dt = \overline{u}_T$ and $b = 12\int_{-T/2}^{T/2} u(t)t\,dt/T^3$ Kristensen (1998) presents the spectral transfer function for this case. When analyzing data for this paper, use of a transfer function based on Eq. (A4) with the rhs normalized by a did not lead to computational difficulties.

REFERENCES

Anderson, D. E., S. B. Verma, R. J. Clement, D. D. Baldocchi, and D. R. Matt, 1986: Turbulence spectra of CO_2, water vapor, temperature and velocity over a deciduous forest. *Agric. For. Meteor.*, **31,** 81–99.

Aubinet, M., and Coauthors, 2000: Estimates of the annual net carbon and water exchange of forests: The EUROFLUX methodology. *Adv. Ecol. Res.*, **30,** 13–175.

Baldocchi, D., 1997: Flux footprints within and over forest canopies. *Bound.-Layer Meteor.*, **85,** 273–292.

——, C. A. Vogel, and B. Hall, 1997: Seasonal variation of energy and water vapor exchange rates above and below a boreal jack pine forest canopy. *J. Geophys. Res.*, **102,** 28 939–28 951.

——, J. Finnigan, K. Wilson, K. T. Paw U, and E. Falge, 2000: On measuring net ecosystem carbon exchange over tall vegetation in complex terrain. *Bound.-Layer Meteor.*, **96,** 257–291.

Barr, A. G., K. M. King, T. J. Gillespie, G. den Hartog, and H. H. Neumann, 1994: A comparison of Bowen ratio and eddy correlation sensible and latent heat flux measurements above deciduous forest. *Bound.-Layer Meteor.*, **71,** 21–41.

Betts, A. K., 1992: FIFE atmospheric boundary layer budget methods. *J. Geophys. Res.*, **97,** 18 523–18 531.

Blackadar, A. K., 1979: High resolution models of the planetary boundary layer. *Environmental Science and Engineering*, J. R. Pfaffin and E. N. Ziegler, Eds., Gordon and Breach, 50–85.

Blanken, P. D., and Coauthors, 1997: Energy balance and canopy conductance of a boreal aspen forest: Partitioning overstory and understory components. *J. Geophys. Res.*, **102,** 28 915–28 927.

——, and Coauthors, 1998: Turbulent flux measurements above and below the overstory of a boreal aspen forest. *Bound.-Layer Meteor.*, **89,** 109–140.

Chen, J. M., P. M. Rech, S. T. Gower, J. M. Norman, and S. Plummer, 1997: Leaf area index of boreal forests: Theory, techniques, and measurements. *J. Geophys. Res.*, **102,** 29 429–29 443.

Desjardins, R. L., and Coauthors, 1997: Scaling up flux measurements for the boreal forest using aircraft–tower combinations. *J. Geophys. Res.*, **102,** 29 125–29 134.

Finnigan, J. J., 1999: A comment on paper by Lee (1998): ''On micrometeorological observations of surface–air exchange over tall vegetation.'' *Agric. For. Meteor.*, **97,** 55–64.

Fitzjarrald, D. R., and K. E. Moore, 1994: Growing season boundary layer climate and surface exchanges in a subarctic lichen woodland. *J. Geophys. Res.*, **99,** 1899–1918.

Foken T., and B. Wichura, 1996: Tools for quality assessment of surface-based flux measurements. *Agric. For. Meteor.*, **78,** 83–105.

Garstang, M., and D. R. Fitzjarrald, 1999: *Observations of Surface to Atmospheric Interactions in the Tropics.* Oxford University Press, 405 pp.

Goulden, M. L., J. W. Munger, S.-M. Fan, B. C. Daube, and S. C. Wofsy, 1996: Effects of interannual climate variability on the carbon dioxide exchange of a temperate deciduous forest. *Science*, **271,** 1576–1578.

——, B. C. Daube, S.-M. Fan, D. J. Sutton, M. Bazzaz, J. W. Munger, and S. C. Wofsy, 1997: Physiological responses of a black spruce forest to weather. *J. Geophys. Res.*, **102,** 28 987–28 996.

Gower, S. T., J. G. Vogel, J. M. Norman, C. J. Kurachick, S. J. Steele,

and T. K. Stow, 1997: Carbon distribution and above ground net primary production in aspen, jack pine, and black spruce stands in Saskatchewan and Manitoba, Canada. *J. Geophys. Res.,* **102,** 29 029–29 041.

Grossman, R. L., 1992: Convective boundary layer budgets of moisture and sensible heat over an unstressed prairie. *J. Geophys. Res.,* **97,** 18 425–18 438.

Hamming, R. W., 1977: *Digital Filters.* Prentice-Hall, 284 pp.

Horst, T. W., and J. C. Weil, 1991: Footprint estimation for scalar flux measurements in the atmospheric surface layer. *Bound.-Layer Meteor.,* **59,** 279–296.

——, and ——, 1994: How far is far enough? The fetch requirements for micrometeorological measurement of surface fluxes. *J. Atmos. Oceanic Technol.,* **11,** 1018–1025.

Jarvis, P. G., J. M. Massheder, S. E. Hale, J. B. Moncrieff, M. Rayment, and S. L. Scott, 1997: Seasonal variation of carbon dioxide, water vapor, and energy exchanges of a boreal black spruce forest. *J. Geophys. Res.,* **102,** 28 952–28 966.

Jork, E. M., and Coauthors, 1998: Long-term carbon dioxide and water vapor flux measurements above a Pacific Northwest Douglas-fir forest. Preprints, *23d Conf. on Agricultural and Forest Meteorology,* Albuquerque, NM, Amer. Meteor. Soc., 99–102.

Kaharabata, S. K., P. H. Schuepp, S. Ogunjemiyo, S. Shen, M. Y. Leclerc, R. L. Desjardins, and J. I. MacPherson, 1997: Footprint considerations in BOREAS. *J. Geophys. Res.,* **102,** 29 113–29 124.

Kaimal, J. C., 1978: Horizontal velocity spectra in an unstable surface layer. *J. Atmos. Sci.,* **35,** 18–25.

——, and J. J. Finnigan, 1994: *Atmospheric Boundary Layer Flows.* Oxford University Press, 289 pp.

——, J. C. Wyngaard, Y. Izumi, and O. R. Coté, 1972: Spectral characteristics of surface layer turbulence. *Quart. J. Roy. Meteor. Soc.,* **98,** 563–589.

Kristensen, L., 1998: Time series analysis. Dealing with imperfect data. Risø National Laboratory Tech. Rep. RISØ-I-1228(EN), 31 pp. [Available from Risø National Laboratory, P.O. Box 49, DK4000 Roskilde, Denmark.]

——, and D. R. Fitzjarrald, 1984: The effect of line averaging on scalar flux measurements with a sonic anemometer near the surface. *J. Atmos. Oceanic Technol.,* **1,** 138–146.

Lafleur, P. M., J. H. McCaughey, D. W. Joiner, P. A. Barlett, and D. E. Jelinski, 1997: Seasonal trends in energy water, and carbon dioxide fluxes at a northern boreal wetland. *J. Geophys. Res.,* **102,** 29 009–29 020.

Laubach, J., and K. G. McNaughton, 1998: A spectrum-independent procedure for correcting eddy fluxes measured with separated sensors. *Bound.-Layer Meteor.,* **89,** 445–467.

Lee, X., 1998: On micrometeorological observations of surface–air exchange over tall vegetation. *Agric. For. Meteor.,* **91,** 39–49.

——, and A. Black, 1993: Atmospheric turbulence within and above a Douglas-fir stand. Part II. Eddy fluxes of sensible heat and water vapor. *Bound.-Layer Meteor.,* **64,** 369–389.

Leuning, R., and J. Moncrieff, 1990: Eddy covariance CO_2 measurements using open and closed path CO_2 analysers: Correction for analyser water vapour sensitivity and damping of fluctuations in air sampling tubes. *Bound.-Layer Meteor.,* **53,** 63–76.

Lu, C. H., and D. R. Fitzjarrald, 1994: Seasonal and diurnal changes in coherent structures over forest. *Bound.-Layer Meteor.,* **69,** 43–69.

Mahrt, L., 1998: Flux sampling errors for aircraft and towers. *J. Atmos. Oceanic Technol.,* **15,** 416–429.

——, J. I. MacPherson, and R. L. Desjardins, 1994: Observations of fluxes over heterogeneous surfaces. *Bound.-Layer Meteor.,* **67,** 345–367.

Massman, W. J., 2000: A simple method for estimating frequency response corrections for eddy covariance systems. *Agric. For. Meteor.,* **104,** 185–198.

McCaughey, J. H., P. M. Lafleur, D. W. Joiner, P. A. Barlett, A. M. Costello, D. E. Jelinski, and M. G. Ryan, 1997: Magnitudes and seasonal patterns of energy, water, and carbon exchanges at a boreal young jack pine forest in the BOREAS northern study area. *J. Geophys. Res.,* **102,** 28 997–29 007.

McMillen, R. T., 1988: An eddy correlation technique with extended applicability to no-simple terrain. *Bound.-Layer Meteor.,* **43,** 231–245.

Moore, C. J., 1986: Frequency response corrections for eddy correlation systems. *Bound.-Layer Meteor.,* **37,** 17–35.

—— and G. Fisch, 1986: Estimating the heat storage in Amazonian tropical forest. *Agric. For. Meteor.,* **38,** 147–168.

Moore, K. E., D. R. Fitzjarrald, R. K. Sakai, M. L. Goulden, J. W. Munger, and S. C. Wofsy, 1996: Seasonal variation in radiative transfer and turbulent exchange at a deciduous forest in central Massachusetts. *J. Appl. Meteor.,* **35,** 122–134.

——, ——, ——, and J. M. Freedman, 2000: Growing season water balance at a boreal jack pine forest. *Water Resources Res.,* **36,** 483–493.

Oke, T. R., 1987: *Boundary Layer Climates.* 2d ed. Routledge, 435 pp.

Pasquill, F., and F. B. Smith, 1983: *Atmospheric Diffusion.* John Wiley and Sons, 437 pp.

Pattey, E., R. L. Desjardins, and G. St.-Amour, 1997: Mass and energy exchanges over a black spruce forest during key periods of BOREAS 94. *J. Geophys. Res.,* **102,** 28 967–28 975.

Rannik, U., and T. Vesala, 1999: Autoregressive filtering versus linear detrending in estimation of fluxes by eddy covariance method. *Bound.-Layer Meteor.,* **91,** 259–280.

Sakai, R. K., 2000: Observational study of turbulent exchange between the surface and canopy layer over several forest types. Ph.D. dissertation, University at Albany, State University of New York, 182 pp.

——, D. R. Fitzjarrald, and K. E. Moore, 1997: Detecting leaf area and surface resistance during transition seasons. *Agric. For. Meteor.,* **84,** 273–284.

Schmid, H. P., 1997: Experimental design for flux measurements: Matching the scales of observations and fluxes. *Agric. For. Meteor.,* **87,** 179–200.

Schuepp, P. H., M. Y. Lecrerc, J. I. MacPherson, and R. L. Desjardins, 1990: Footprint predictions of scalar fluxes from analytical solutions of the diffusion equation. *Bound.-Layer Meteor.,* **50,** 355–373.

Sun, J., and Coauthors, 1997: Lake induced atmospheric circulations during BOREAS. *J. Geophys. Res.,* **102,** 29 155–29 166.

Webb, E. K., G. I. Pearman, and R. Leuning, 1980: Correction flux measurement for density effects due to heat and water vapour transfer. *Quart. J. Roy. Meteor. Soc.,* **106,** 85–100.

Wofsy, S. C., M. L. Goulden, J. W. Munger, S.-M. Fan, P. S. Bakwin, B. C. Daube, S. L. Bassow, and F. A. Bazzaz, 1993: Net exchange of CO_2 in a mid-latitude forest. *Science,* **260,** 1314–1317.

Wyngaard, J. C., and O. R. Coté, 1972: Cospectral similarity in the atmospheric surface layer. *Quart. J. Roy. Meteor. Soc.,* **98,** 590–603.